Seeking leptoquarks in the $t\bar{t}$ plus missing energy channel at the high-luminosity LHC

Natascia Vignaroli[*]

Istituto Nazionale di Fisica Nucleare, Sezione di Padova, via Marzolo 8, I-35131 Padova, Italy

The $t\bar{t}$ plus missing energy channel is one of the most efficient to detect third-generation leptoquarks (LQs). It offers an important test to models which explain flavor anomalies in B meson decays. We outline a search strategy in the channel, relying on tagging the tops and on observables constructed out of the tops, and we assess the reach on LQs of the future high-luminosity LHC program. We find that with 3 ab^{-1} a vector (scalar) LQ decaying 50% (100%) to top and neutrino can be excluded up to masses of 1.96 TeV (1.54 TeV). We also indicate several observables that, in case of a future discovery in the channel, can be used to distinguish a scalar LQ from a vector LQ. The implications of our findings to models addressing the recent flavor anomalies are finally discussed.

I. INTRODUCTION

Leptoquarks (LQs), which are hypothetical particles carrying both lepton and baryon number, appear in a variety of theories beyond the Standard Model (BSM), as Pati-Salam model [1], grand unification theories [2], and BSM composite dynamics [3]. Recently, third-generation LQs caught special attention from the high-energy physics community, since they represent the best candidates [4–9] to explain anomalies in flavor physics observed by experiments on B meson decays: Belle [10–13], *BABAR* [14,15], and by LHCb [16–18]. In particular, the experiments find the indication of lepton flavor universality violation in the rather clean ratio observables $R_{D^{(*)}}$, at about 4σ level (by combining the results of the different experiments), and $R_{K^{(*)}}$, again at about 4σ level. It is really appealing that the anomalies can be explained simultaneously by models with LQs in the TeV range [19], thus in the reach of the large hadron collider (LHC). Furthermore, some models with LQs can also address the discrepancy from the Standard Model (SM) in the muon magnetic moment [20–22]. The optimization of the search strategies for LQs at the LHC is thus very important to unveil the physics behind the flavor anomalies and in general for seeking BSM physics.

The general LQ phenomenology at hadron colliders has been explored in [23] and more recently in [24–26]. The relevant production mechanisms at the LHC are pair production driven by QCD interactions and single production mediated by model-dependent couplings of the LQs to leptons and quarks. Another possibility to detect the LQs is by analyzing high-p_T dilepton distributions, whose tails can be affected by the t-channel exchange of LQs, mediated by model-dependent couplings [27]. Several searches, which give bounds on the LQ masses, have been performed by ATLAS and CMS in the pair production channel at the 13 TeV LHC [28–33], while the study in [34] considers the single production of third-generation LQs decaying into $b\tau$. Limits can also be obtained by recasting the results of the searches for supersymmetry. The strongest limits on 2/3-charged third-generation LQs are currently set by the CMS analysis in [29], which used 35.9 fb^{-1} of data at a center-of-mass energy $\sqrt{s} = 13$ TeV. Reference [29] reinterprets the results of a search for gluinos and squarks to constraint pair-produced LQs decaying into a neutrino plus a top, a bottom, or a light jet. A vector LQ decaying 50% to $t\nu$ is excluded by this analysis for masses below 1530 GeV in the Yang-Mills (YM) case and for masses below 1115 GeV in the minimal coupling (MC) scenario. A scalar LQ decaying 100% to $t\nu$ is excluded up to masses of 1020 GeV. In our study we will try to improve the search strategy applied in this search and we will estimate the sensitivity of the LHC at a collision energy of 14 TeV and at high luminosity.

Projections of the reach of the High-Luminosity LHC (HL-LHC) and future colliders [35] on different types of LQs have been presented in [36], considering pair production in the $\mu\mu jj$ channel, in [37] for pair and single production in the $b\mu\mu$ and $bb\mu\mu$ channel, and in [38] for a scalar LQ in the $bb\nu\nu$ and $cc\tau\tau$ channel. Estimates of the HL-LHC reach on LQs, based on an extrapolation of the results of current experimental searches, have been also

shown in [39,40]. A recent study has also analyzed the HL-LHC reach on a vector LQ in the $t\bar{t}$ plus missing energy channel [41]. Despite considering the same final state, our analysis and search strategy will be different, relying more on the identification of the tops.

In our study we consider pair-produced vector and scalar LQs each decaying into a top and a neutrino, leading to a final state of two tops plus missing energy. This channel, due to a peculiar topology and to the possibility of exploiting the top tagging to disentangle the signal from the background, proves to be very powerful and, as we will show, it represents one of the best channels to probe LQs involved in the explanation of the flavor anomalies. We outline a search strategy which relies on tagging the two tops in the final state, indicate the HL-LHC reach, and point out several observables, that in case of a future observation of the LQ signal can distinguish between a scalar and a vector LQ. Finally, we present implications of our results to models that explain the recent flavor anomalies.

The paper is organized as follows: We define our model setup in Sec. II, we define our search strategy in Sec. III, and present our results in Sec. IV. Shape observables to distinguish between scalar and vector LQs are shown in Sec. V. In Sec. VI we discuss the implications of our findings to the flavor anomalies. We offer our conclusions in Sec. VII.

II. SETUP

LQ states can be classified [24,42] in terms of their spin (scalar or vector) and SM quantum numbers $[SU(3)_c, SU(2)_L, U(1)_Y]$, where the electric charge $Q = Y + T_3$ is the sum of the hypercharge (Y) and the third component of the weak isospin (T_3). In scenarios with baryon number violating couplings, these particles need to be very heavy in order to avoid the stringent limits on the proton lifetime. On the other hand, if baryon number symmetry is respected, LQ masses and couplings need to satisfy much weaker constraints, allowing them to be considerably lighter. The phenomenology of LQs with $\mathcal{O}(1 \text{ TeV})$ masses is very rich, including potential signatures in flavor physics observables and in the direct searches performed at the LHC.

In this paper we are interested in the $t\bar{t}$ plus missing energy signature at the LHC. This process can be induced by pair-produced LQs, which then decay to a top quark and a neutrino. The production mechanism is dominated by gluon fusion and $q\bar{q}$ annihilation as illustrated in Fig. 1, which, for the scalar LQ, depends on a single parameter, the LQ mass. The vector LQ QCD production is controlled by a second parameter k, which describes nonminimal interactions of U_1 with gluons and depends on underlying dynamics. The branching fraction ($\mathcal{B}$) for LQ → $t\bar{\nu}$ is model dependent. In Table I, we list the LQ states that can decay to $t\bar{\nu}$, along with the corresponding operator, which can arise via interactions with a lepton doublet (L) or
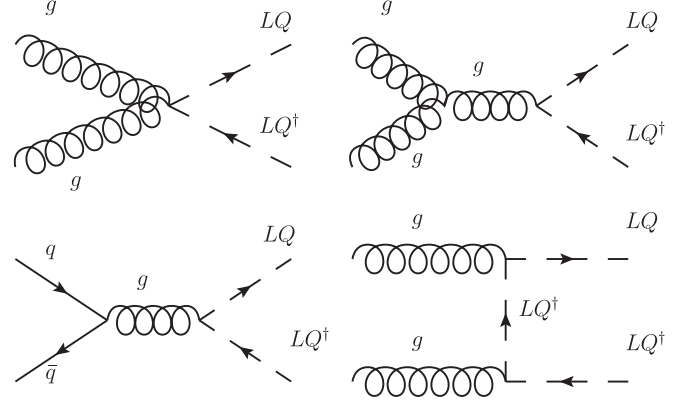

FIG. 1. Leading diagrams for the pair production of LQs at the LHC.

a right-handed neutrino (ν_R). Depending on the type of interaction and the $SU(2)_L \times U(1)_Y$ LQ representation, one can derive the maximal value of $\mathcal{B}(\text{LQ} \to t\bar{\nu})$ allowed by gauge symmetry, as listed in the third column of Table I. This branching fraction can be as large as 50% or 100% for interactions with left-handed doublets, depending if the Yukawa coupling contributing to this also enters in the $SU(2)$ counterpart, but it can be as large as 100% if interactions with right-handed neutrinos are allowed.

Our analysis will be performed with two representative models, which can produce the same final state. Motivated by the B-physics anomalies, we consider: (i) the scalar LQ $S_3 = (\bar{\mathbf{3}}, \mathbf{3}, 1/3)$ and the (ii) vector LQ $U_1 = (\mathbf{3}, \mathbf{1}, 2/3)$, which we describe now in detail.

TABLE I. Classification of the LQ states that can decay to $t\bar{\nu}$, in terms of the SM quantum numbers $[SU(3)_c, SU(2)_L, Y]$, with $Q = Y + T_3$. We adopt the same notation of Ref. [24] and we omit color, weak isospin, and flavor indices for simplicity. The last column corresponds to the maximal value of $\mathcal{B}(\text{LQ} \to t\bar{\nu})$, as allowed by gauge symmetries. In the cases where interactions to lepton doublets (L) and right-handed neutrinos (ν_R) are both allowed, i.e., for the models U_1 and $\tilde{V}_2$, we give the maximal branching fraction assuming only interactions to L or ν_R, respectively.

Field	Spin	Quantum numbers	Operators	$\mathcal{B}(\text{LQ} \to t\bar{\nu})$
R_2	0	$(\mathbf{3}, \mathbf{2}, 7/6)$	$\overline{u_R} R_2 i\tau_2 L$	≤ 0.5
$\widetilde{R}_2$	0	$(\mathbf{3}, \mathbf{2}, 1/6)$	$\bar{Q} \widetilde{R}_2 \nu_R$	≤ 1
$\bar{S}_1$	0	$(\bar{\mathbf{3}}, \mathbf{1}, -2/3)$	$\overline{u_R^C} \bar{S}_1 \nu_R$	≤ 1
S_3	0	$(\bar{\mathbf{3}}, \mathbf{3}, 1/3)$	$\overline{Q^C} i\tau_2 \vec{\tau} \cdot \vec{S}_3 L$	≤ 1
U_1	1	$(\mathbf{3}, \mathbf{1}, 2/3)$	$\bar{Q}\gamma_\mu U_1^\mu L$, $\overline{u_R}\gamma_\mu U_1^\mu \nu_R$	$\leq 0.5, 1$
$\tilde{V}_2$	1	$(\bar{\mathbf{3}}, \mathbf{2}, -1/6)$	$\overline{u_R^C}\gamma_\mu \tilde{V}_2^\mu i\tau_2 L$, $\overline{Q^C}\gamma_\mu i\tau_2 \tilde{V}_2^\mu \nu_R$	$\leq 0.5, 1$
U_3	1	$(\mathbf{3}, \mathbf{3}, 2/3)$	$\bar{Q}\gamma_\mu \vec{\tau} \cdot \vec{U}_3^\mu L$	≤ 0.5

(1) $S_3 = (\bar{\mathbf{3}}, \mathbf{3}, 1/3)$

This S_3 LQ has been considered in models addressing the B-physics anomalies with two scalar LQs [39,43]. The Yukawa Lagrangian of this model reads [24]

$$\mathcal{L}_{S_3} = y_L^{ij} \overline{Q_i^C} i\tau_2 (\tau_k S_3^k) L_j + \text{H.c.}, \qquad (1)$$

where τ_k ($k = 1, 2, 3$) denote the Pauli matrices, S_3^k are the LQ triplet component, and y_L is a generic Yukawa matrix. Note that we have neglected LQ couplings to diquarks in the above equation since they would disturb the proton stability [24]. An appropriate symmetry must be imposed to forbid these couplings, which are tightly constrained by experimental limits on the proton lifetime. It is convenient to recast the above expression in terms of charge eigenstates, namely,

$$\begin{aligned}\mathcal{L}_{S_3} = &-y_L^{ij} \overline{d_{Li}^C} \nu_{Lj} S_3^{(1/3)} - \sqrt{2} y_L^{ij} \overline{d_{Li}^C} \ell_{Lj} S_3^{(4/3)} \\ &+ \sqrt{2}(V^* y_L)^{ij} \overline{u_{Li}^C} \nu_{Lj} S_3^{(-2/3)} \\ &- (V^* y_L)^{ij} \overline{u_{Li}^C} \ell_{Lj} S_3^{(1/3)} + \text{H.c.}, \end{aligned} \qquad (2)$$

where V is the Cabibbo-Kobayashi-Maskawa matrix.[1] The superscript denotes the electric charge of the LQ states. In this particular model, the branching fraction we are interested in reads

$$\mathcal{B}(S_3^{(2/3)} \to t\bar{\nu}) \simeq \frac{(y_L \cdot y_L^\dagger)_{33}}{\sum_i (y_L \cdot y_L^\dagger)_{ii}}, \qquad (3)$$

where we have neglected the fermion masses and used the fact that $|V_{tb}| \gg |V_{ts}| \gg |V_{td}|$. We adopted a compact notation where $(y_L \cdot y_L^\dagger)_{ii} \equiv \sum_j |y_L^{ij}|^2$.

(2) $U_1 = (\mathbf{3}, \mathbf{1}, 2/3)$

The U_1 model attracted a lot of attention because it can provide a simultaneous explanation to the anomalies in $b \to s$ and $b \to c$ transitions, with a single mediator [40]. The most general Lagrangian consistent with the SM gauge symmetry allows couplings to both left- and right-handed fermions, namely,

$$\begin{aligned}\mathcal{L}_{U_1} = &x_L^{ij} \bar{Q}_i \gamma_\mu U_1^\mu L_j + x_R^{ij} \bar{d}_{Ri} \gamma_\mu U_1^\mu \ell_{Rj} \\ &+ w_R^{ij} \bar{u}_{Ri} \gamma_\mu U_1^\mu \nu_{Rj} + \text{H.c.}, \end{aligned} \qquad (4)$$

where x_L^{ij}, x_R^{ij}, and w_R^{ij} are Yukawa couplings. If we neglect the interactions to right-handed fields, we have, in the mass eigenstate basis,

$$\mathcal{L}_{U_1}^L = (V^* x_L)^{ij} \bar{u}_{Li} \gamma_\mu U_1^\mu \nu_{Lj} + x_L^{ij} \bar{d}_{Li} \gamma_\mu U_1^\mu \ell_{Lj} + \text{H.c.} \qquad (5)$$

and we obtain that

$$\mathcal{B}(U_1^{(2/3)} \to t\bar{\nu}) \simeq \mathcal{B}(U_1^{(2/3)} \to b\bar{\tau}) \simeq \frac{1}{2} \frac{(x_L \cdot x_L^\dagger)_{33}}{\sum_i (x_L \cdot x_L^\dagger)_{ii}}, \qquad (6)$$

where we neglected fermion masses, similar to Eq. (3).

The U_1 QCD interactions that control the U_1 pair production are determined by the kinetic terms

$$\mathcal{L}^{\text{kin}} = -\frac{1}{2} U_1^{\dagger \mu\nu} U_{\mu\nu}^1 - ig_s k U_1^{\dagger \mu} T^a U_1^\nu G_{\mu\nu}^a, \qquad (7)$$

where $U_1^{\mu\nu}$ denotes the U_1 strength tensor and k is a dimensionless parameter which depends on the ultraviolet completion of the model. We can identify the two scenarios of MC, $k = 0$, and the YM case $k = 1$.

In the following, we will assume that the dominant interactions are the ones to third-generation left-handed fermions, as suggested by the B-physics anomalies. In this case, the branching fractions to $t\nu$ will be 100% for S_3 and 50% for U_1, which are the most optimistic values. Nonetheless, it is clear that our results can be rescaled and applied to more general flavor structures and to the other models listed in Table I.

III. SEARCH STRATEGY

We outline a search strategy at the 14 TeV LHC for pair-produced scalar and vector LQs, decaying each into a top quark and a neutrino. In particular, we will consider the U_1 and S_3 LQs introduced in Sec. II, assuming a decay branching ratio into $t\nu$ of 50% for U_1 and of 100% for S_3. For U_1, we will analyze the YM scenario $k = 1$. At the end, we will also present the HL-LHC reach in the MC scenario, $k = 0$, which will be calculated based on the efficiencies obtained in our analysis and by rescaling the signal number of events according to the different values of the production cross sections. Figure 2 shows cross section values at the 14 TeV LHC for the QCD pair production of S_3 and U_1 in both the YM and MC cases.

We focus on a final state given by two tops decaying hadronically plus missing energy. The main background consists of $Z +$ jets events, where the Z decays to neutrinos and leads to missing energy. Minor backgrounds, which we also include in our analysis, come from $W +$ jets and $t\bar{t}$ events, where a leptonic decaying W leads to missing energy from the neutrino and a lost lepton [29].[2]

---

[1]The Pontecorvo-Maki-Nakagawa-Sakata matrix is not relevant to our study and has been set to the identity [25].

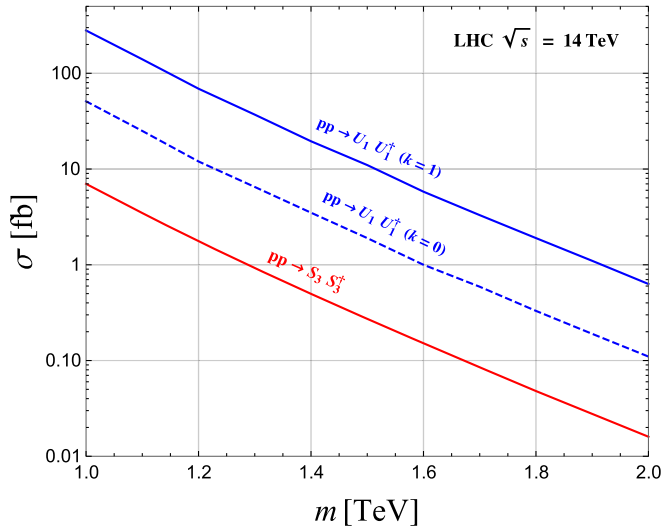[2]We checked that other backgrounds, as QCD multijet events, give a negligible contribution.

FIG. 2. Cross section values at the 14 TeV LHC for the QCD pair production of vector (blue line) and scalar (red line) LQs. For the vector U_1, we indicate the cross sections in both the minimal coupling $k = 0$ (dashed line) and the Yang-Mills $k = 1$ (continuous line) scenarios. The cross sections are calculated at (next-to-)leading order in QCD for the (scalar) vector LQ.

We simulate signal and background events at leading order with MadGraph5_aMC@NLO [44]. Events are then passed to PYTHIA [45] for showering and hadronization. We also apply a smearing to the jet momenta in order to mimic detector effects [46]. Signal events are generated via UFO files [47], created by using FeynRules [48]. For the case of the scalar LQ S_3, we apply correction factors to the cross section values, which account for QCD next-to-leading-order effects.[3] We calculate them by using the code in Ref. [25] (see also Ref. [49]), with the choice of the NN23NLO parton distribution function (PDF) set [50], $\alpha_S = 0.122$ and dynamical factorization and renormalization scales. The same α_S and scale values are used in the leading-order simulations, with the choice of the NN23LO1 PDF set [50]. Jets are clustered with FastJet [51] by using an anti-kt algorithm [52]. We choose a large cone size, $R = 1.0$, which we identify as an optimal choice, based on the top reconstruction procedure which we will apply.[4]

The signal we want to detect is characterized by large missing transverse energy, $\not{E}_T$, and at least two fat jets, coming from the hadronic decays of the two tops.

Considering these signal features, as a first step of our analysis, we accept the events if they satisfy the conditions

$$\not{E}_T > 250 \text{ GeV},$$
$$n_j \geq 2(p_T j > 30 \text{ GeV}, |\eta_j| < 5), \quad \text{lepton veto}, \quad (8)$$

with n_j denoting the number of jets satisfying the p_T and rapidity requirements in the parentheses. Events are rejected if at least one isolated lepton, either a muon or an electron, with $p_T > 10$ GeV and in the central region $|\eta| < 2.5$ is found (lep veto).[5]

A crucial part of our search strategy relies on the reconstruction of both of the two tops in the final state. To reconstruct the top pair we apply the following procedure. We first consider the invariant mass of the leading jet. Since the jets are clustered on a relatively large cone size and the tops in the signal are boosted, most of the top decay products are collected in a single fat jet. As we can see from the plot on the left in Fig. 3, the invariant mass of the p_T-leading jet, $j(1)$, is centered around the top mass for a large portion of the signal events. As a first step of the reconstruction procedure we thus select the events with the $j(1)$ invariant mass, $M_{j(1)}$, in the region (160, 220 GeV). $j(1)$ is then identified with the p_T-leading top, $t(1)$. We then analyze the invariant mass of the second-leading jet. As evident from the plot on the right in Fig. 3, the majority of signal events are again centered around the top mass. If $M_{j(2)}$ is within the region (160, 220 GeV) we identify the second-leading top, $t(2)$, with $j(2)$. A small portion of signal events for $M_{j(2)}$ is centered around the W mass. In order to retain these signal events we consider the $j(2)$ invariant mass region (70, 110 GeV) and the system given by the second and the third p_T-leading jets. If the invariant mass of the $j(2)$ plus $j(3)$ system is within the interval (160, 220 GeV) the system is identified with $t(2)$. We select the events where both of the two tops, $t(1)$ and $t(2)$, have been identified with the outlined procedure. The efficiency of our top pair tagging is about 20% for the signal, while we can reject the background by a factor of about 1.4×10^3. Table II indicates the cross section values for signal and background after the acceptance cuts and after the reconstruction and tagging of the pair of top quarks.

Once having identified the tops $t(1)$ and $t(2)$, we construct several observables based on them, which efficiently discriminate the LQ signals from the background. We will thus complete our signal selection by applying cuts on these "top observables." One of these observables, that we indicate by M_{T2}, is inspired by the M_{T2} variable commonly used by experimental searches [56]. In our study

---

[3]K-factors are included only for S_3. The calculations for U_1 are at tree level (due to the ambiguity in the ultraviolet completion of the model).

[4]In our simulations we do not include initial state radiation or underline events. This is because, as proved for example in [53], the effects of contamination on the jet invariant mass coming from these events can be eliminated by applying techniques as "grooming" [54]. We thus expect that our simulations can correctly reproduce the distributions that an experimental analysis can find after the application of these advanced jet "cleaning" techniques.

[5]We consider the lepton isolated if it is separated from a jet by $\Delta R > 0.4$. The choice of 10 GeV as a trigger on the lepton p_T is a conservative choice for the evaluation of the $W +$ jets and $t\bar{t}$ background contribution. Indeed, the current ATLAS trigger is 7 GeV for electrons and 6 GeV for muons [55].
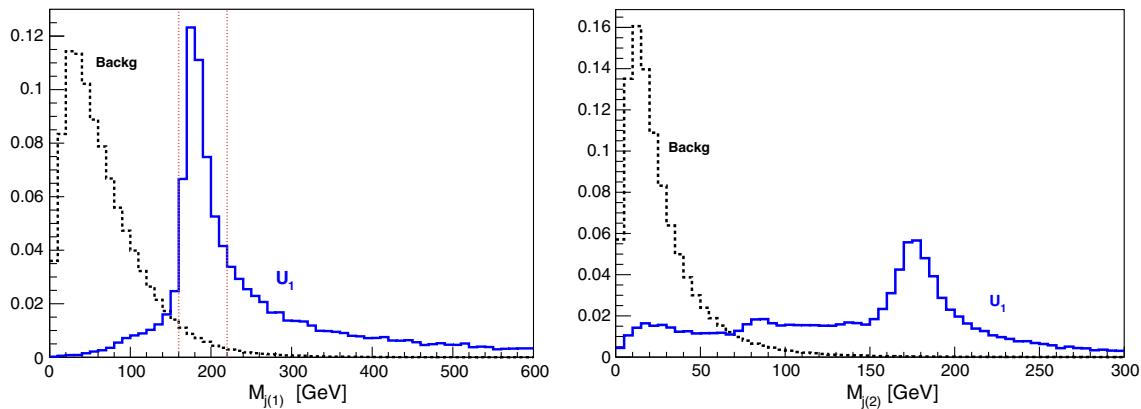
FIG. 3.   Normalized distributions for background and a signal from a LQ U_1 of 1.7 TeV (in the YM case). (Left) Invariant mass of the p_T-leading jet. The red dotted lines mark the window around the top mass considered in this analysis. (Right) Invariant mass of the second-leading jet.

it is constructed upon the tops, instead of on jets, and it is defined as

$$M_{T2} \equiv \max\{M_{Tt(1)}, M_{Tt(2)}\},$$
$$M_{Tt(i)} = \sqrt{2\not{E}_T p_T t(i)(1 - \Delta\phi(\not{E}, t(i))/\pi)}, \quad i = 1, 2, \qquad (9)$$

where $p_T t(1,2)$ is the transverse momentum of the top $t(1,2)$ and $\Delta\phi(\not{E}, t(1,2))$ denotes the azimuthal angular separation between the missing energy vector and the top $t(1,2)$. We then consider as a signal-to-background

discriminant the invariant mass of the system made of the two tops $t(1)$ and $t(2)$, which we indicate as M_{tt}.

After the top reconstruction we thus refine our signal selection by imposing the cuts

$$\not{E}_T > 500 \text{ GeV}, \qquad M_{tt} > 800 \text{ GeV}, \qquad (10)$$

which exploits the large missing energy and the large invariant mass of the top pair system in the signal events and the two set of cuts on the transverse momenta of the tops and on the M_{T2} variable

$$\text{loose: } M_{T2} > 800 \text{ GeV} \quad p_T t(1) > 500 \text{ GeV} \quad p_T t(2) > 300 \text{ GeV},$$
$$\text{tight: } M_{T2} > 1100 \text{ GeV} \quad p_T t(1) > 700 \text{ GeV} \quad p_T t(2) > 500 \text{ GeV}, \qquad (11)$$

TABLE II.   Cross section values at the 14 TeV LHC after the acceptance cuts (columns on the left) and the identification of the pair of top quarks (columns on the right).

	Acceptance				Top tagging		
U_1 (YM)		S_3		U_1 (YM)		S_3	
m (TeV)	σ (fb)	m (TeV)	σ (fb)	m (TeV)	σ (fb)	m (TeV)	σ (fb)
1.6	0.45	1.1	1.4	1.6	0.097	1.1	0.23
1.7	0.26	1.2	0.71	1.7	0.056	1.2	0.13
1.8	0.15	1.3	0.38	1.8	0.032	1.3	0.073
1.9	0.084	1.4	0.21	1.9	0.019	1.4	0.042
2.0	0.050	1.5	0.11	2.0	0.011	1.5	0.024
2.1	0.030	1.6	0.064	2.1	0.0068	1.6	0.013
		σ (fb)				σ (fb)	
	$Z + jets$	4560			$Z + jets$	3.02	
	$W + jets$	1330			$W + jets$	0.86	
	$t\bar{t}$	95			$t\bar{t}$	0.36	
	Total background	5990			Total background	4.24	

TABLE III.   Cross section values at the 14 TeV LHC after the final selection. The tight (loose) selection in Eq. (11) has been applied to signals with masses above (up to) 1.4 TeV.

U_1 (YM)					
m (TeV)	1.6	1.7	1.8	1.9	2.0	2.1
σ (fb)	0.047	0.030	0.019	0.011	0.0072	0.0045
S_3					
m (TeV)	1.1	1.2	1.3	1.4	1.5	1.6
σ (fb)	0.12	0.074	0.047	0.028	0.011	0.0066
Background		loose			tight	
σ (fb)		0.25			0.080	

where the loose (tight) selection is applied to signals with masses up to (above) 1.4 TeV. Signal and background distributions for the relevant observables used in this analysis are shown in Fig. 5.

Table III presents the cross section values for signal and background after the complete selection, namely after the top tagging plus the cuts in Eq. (10) and the loose or tight selection in (11).

IV. HL-LHC REACH

Based on our final results, shown in Table III, we calculate the HL-LHC reach on LQs. In particular, we derive the values for the integrated luminosity needed to exclude at 95% confidence level (C.L.) or to observe at 3σ a scalar LQ S_3 and a vector LQ U_1 as a function of their mass. The exclusion reach at 95% C.L. is calculated by a goodness-of-fit test considering a Poisson distribution for the events. The 3σ reach is estimated according to the significance level $S/\sqrt{B}$, with S (B) the number of signal (background) events.

Figure 4 shows the HL-LHC reach on vector and scalar LQs. We see that with 3 ab^{-1} (300 fb^{-1}) the HL-LHC can
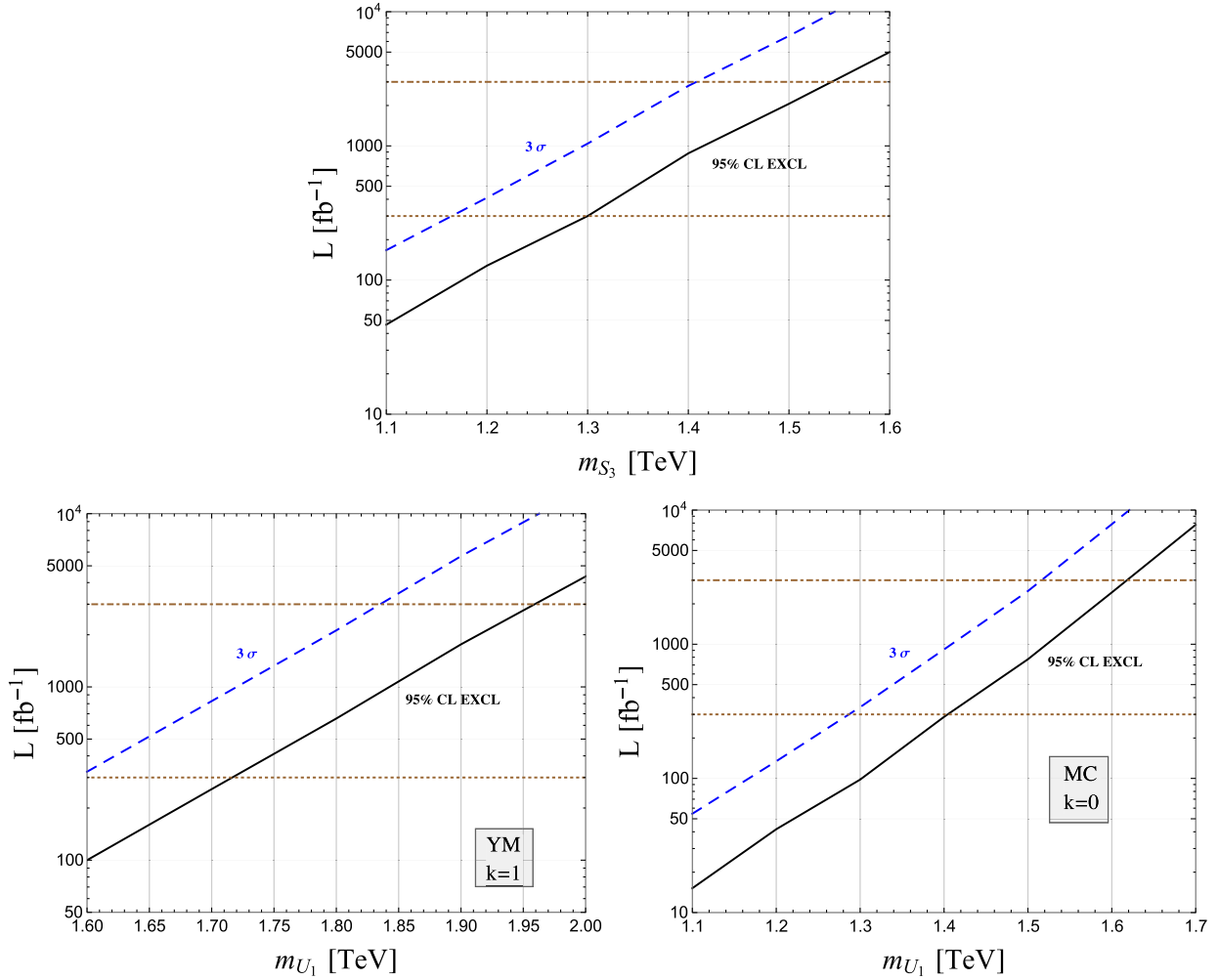

FIG. 4.   HL-LHC reach. Integrated luminosity required to exclude at 95% C.L. (black line) or to observe at 3σ (blue dashed line) a scalar LQ S_3 (upper plot) and a vector LQ U_1 (lower plots) as a function of their mass. For U_1, the plot on the left (right) refers to the YM (MC) scenario with $k = 1(0)$.

exclude a vector LQ U_1 up to 1.96 TeV (1.72 TeV) or observe at 3σ the corresponding signal for masses up to 1.83 TeV (1.6 TeV) in the YM case. In the MC scenario, U_1 LQs up to 1.62 TeV (1.4 TeV) can be excluded with 3 ab^{-1} (300 fb^{-1}). For the scalar LQ S_3, the exclusion reach extends up to 1.54 TeV (1.3 TeV) with 3 ab^{-1} (300 fb^{-1}), while S_3 as heavy as 1.41 TeV (1.16 TeV) can be observed at 3σ.

The reach for a scalar LQ S_3 can be confronted with the expected reach obtained by extrapolating the results of the CMS analysis [29], which has been presented in [39]. The corresponding bounds are $m_{S_3} > 1.43$ (1.2) TeV with 3 ab^{-1} (300 fb^{-1}). The CMS study makes use of variables as missing energy and other based on the p_T of jets in the final state, but does not apply any top tagging. Given the fact that the reach of our analysis is considerably larger than the one in Ref. [39],[6] we point out that the identification of the tops in the final state and the use of "top observable" for the signal-to-background discrimination can improve the LHC sensitivity to LQs. Furthermore, in our study we have applied a simple cut-and-count analysis and we expect our results to be conservative. A more refined top reconstruction, making use for example of substructure techniques such as "jettiness" [57,58] or a statistical analysis of the shape of the relevant distributions considered in this study (see the subsequent Sec. V), could augment the reach of the HL-LHC. We leave these analyses to a more specialized experimental work.

V. DISTINGUISHING BETWEEN SCALAR AND VECTOR LEPTOQUARKS

We consider here the case where the HL-LHC will discover a LQ signal in the channel analyzed in this study, following the search strategy outlined in Sec. III. We discuss in this section how to distinguish between the two possible signals of a vector LQ and a scalar LQ.

We indicate several observables that can be used to distinguish between the two cases. A first category of observables uses the difference in the energy of the final states coming from a scalar or a vector LQ. Indeed, due to the different scaling of the QCD pair production cross section with the mass, LQ signals from a vector LQ and a scalar one, where the vector is considerably heavier than the scalar LQ, can be identified with a similar significance. For example, considering our results, we find that with 3 ab^{-1} a 5σ discovery could be realized for either a vector LQ U_1, in the YM case, of about 1.7 TeV ($S/\sqrt{B} = 5.8$) or a lighter scalar S_3 of about 1.3 TeV ($S/\sqrt{B} = 5.1$). The observables we identify are constructed from the reconstructed pair of

tops. Tagging the two tops is thus important not only to discover the LQs but also to characterize the signal.

The top observables M_{tt}, M_{T2}, and the p_T of the two tops that we already used to disentangle the signal from the background can also efficiently distinguish between U_1 and S_3. An other observable we point out as a signal analyzer is an angular observable, specifically the azimuthal angular separation between the two reconstructed tops. $\Delta\phi(tt)$ is sensible in a nontrivial way to spin correlations[7] and it is thus able to probe "directly" the spin of the LQs.[8] Similar observables, but for different topologies and constructed from the leptonic decays of tops, have been considered to identify properties of dark matter interactions [60,61] and of Higgs couplings [62,63].

Figure 5 shows the distribution of the top observables for the background and the scalar and vector LQ signals. They have been obtained after the procedure of top tagging and after applying the cuts: $\not{E}_T > 500$ GeV, $M_{tt} > 800$ GeV. We can see that the signal from U_1 is distributed on larger values of the top observables compared to the signal from S_3. The difference is particularly clear in the tails of the distributions.[9]

Figure 6 shows the $\Delta\phi(tt)$ distribution for the background and the U_1 and S_3 signals. The background tends to be more homogeneously distributed, the vector signal is characterized by tops at larger azimuthal separation compared to the scalar case. The difference in the $\Delta\phi(tt)$ shape depends on the spin of the LQs and does not change significantly with other values of the LQ masses, different from the other top observables discussed above. $\Delta\phi(tt)$ is thus particularly helpful to distinguish between the signals from a scalar LQ S_3 and a vector U_1 in the MC scenario $k = 0$, where the differences in the energy of the final states are less marked.

As a final remark, we point out that a complementary way to distinguish between different LQs could be to search for specific signatures which are present for a type of LQ and not for the others. In our scenario, for example, the vector U_1, different from S_3, could be detectable in searches with a $b\tau$ final state, as $bb\tau\tau$, $tb\tau + \not{E}_T$, or $b\tau+$ jets.

VI. IMPLICATIONS TO THE FLAVOR ANOMALIES

LQs with masses in the TeV range are particularly interesting, since they can mediate flavor-violating processes that can accommodate the deviations from the

---

[6]The reach in [39] is calculated by assuming a center-of-mass energy of 13 instead of 14 TeV. We calculate that the reach of our analysis remains significantly larger even if we rescale the cross sections according to the different $\sqrt{s}$.

[7]See [59] for a study of spin correlations in the azimuthal angular separation of decay products.
[8]Different from the other top observables, that can distinguish the spin "indirectly," through the different scaling of the production cross section with the mass for vector and scalar LQs.
[9]In this section we just point out the relevant observables and show the corresponding distributions. A statistical analysis based on the different shapes of the distributions is beyond the scope of the present work.
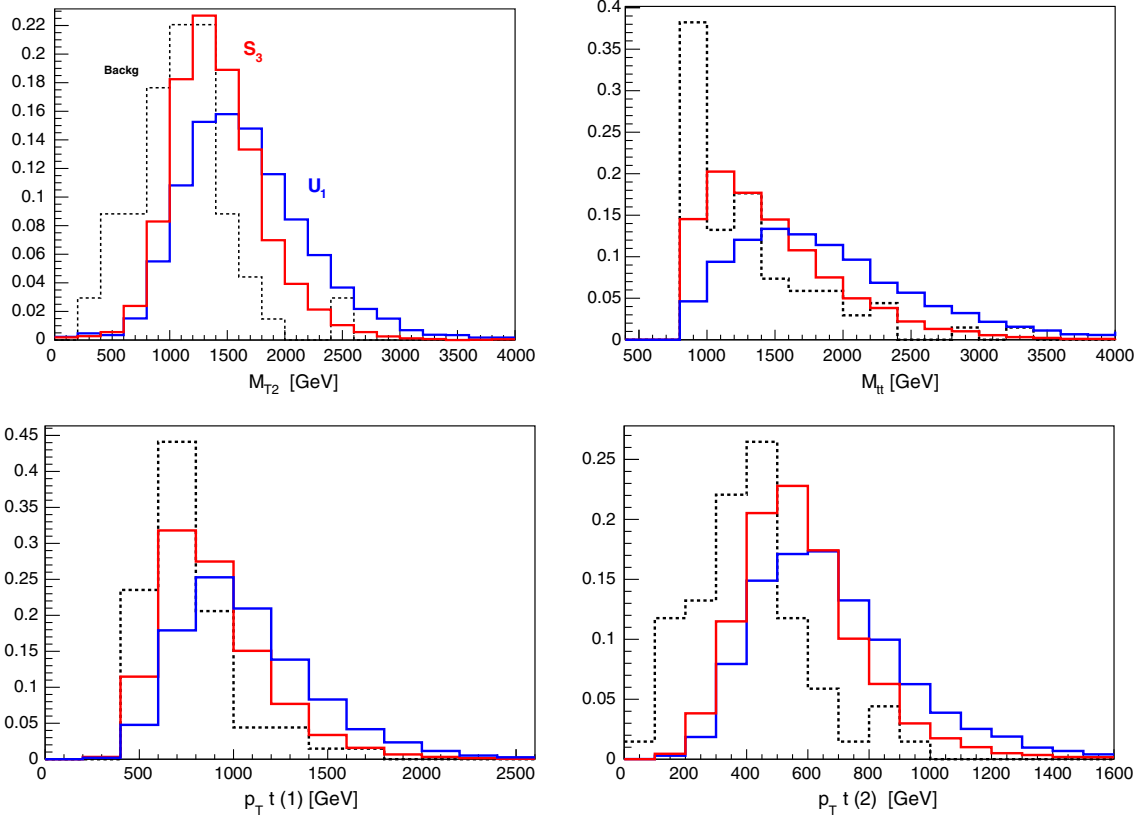
FIG. 5. Normalized distributions of top observables for the background (black dotted curve) and the signals from a scalar LQ S_3 of 1.3 TeV (red curve) and from a vector LQ U_1 of 1.7 TeV with $k = 1$ (blue curve). The tagging of the tops and the following cuts are applied: $\not{E}_T > 500$ GeV, $M_{tt} > 800$ GeV. (Left, upper) Distributions of the M_{T2} variable as defined in Eq. (9). (Right, upper) Invariant mass distributions of the reconstructed top pair. [Left (right), lower] p_T distribution of the reconstructed leading (second leading) top.
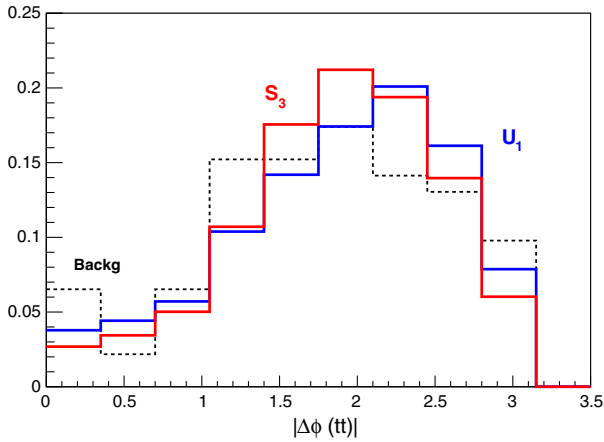
FIG. 6. Normalized distributions of the azimuthal angular separation between the two reconstructed tops for the background (black dotted curve) and the signals from a scalar LQ S_3 of 1.3 TeV (red curve) and from a vector LQ U_1 of 1.7 TeV with $k = 1$ (blue curve). The top tagging procedure and the following cuts are applied: $\not{E}_T > 500$ GeV, $M_{tt} > 800$ GeV.

Standard Model observed in the decays of B mesons. In particular, the deviations are measured in the observables $R_{D^{(*)}} \equiv \frac{\mathcal{B}(B \to D^{(*)}\tau\bar{\nu})}{\mathcal{B}(B \to D^{(*)}\ell\bar{\nu})}$, with $\ell \equiv \mu, e$, and $R_{K^{(*)}} \equiv \frac{\mathcal{B}(B \to K^{(*)}\mu^+\mu^-)}{\mathcal{B}(B \to K^{(*)}e^+e^-)}$.

In this section we compare the reach on LQs derived in our study for the HL-LHC with the regions of parameters favored by the B-physics anomalies.

First, we consider the model with a vector $SU(2)_L$ singlet. This simplified model is particularly attractive because it allows for a simultaneous explanation of the B-physics anomalies, both in $R_{D^{(*)}}$ and $R_{K^{(*)}}$, with a single particle, the LQ U_1 (cf. [64] for a recent review). We adopt the ansatz of Ref. [40], which is based on a $U(2)_q \times U(2)_\ell$ minimally broken flavor symmetry controlling the light generation couplings. In this case, we have, for the couplings in Eq. (4), $x_L^{ij} \equiv g_U \beta_{ij}$, with $\beta_{ij} = \delta_{3i}\delta_{3j}$ up to small breaking terms of the flavor symmetry. Reference [40] calculated the region in the plane coupling vs mass favored by B-physics anomalies. We show in Fig. 7 which part of this region can be probed by our analysis in the $t\bar{t}\nu\nu$ channel at the HL-LHC. The plot on the left refers to the YM scenario for the QCD pair production of U_1, the plot on the right refers to the MC case.
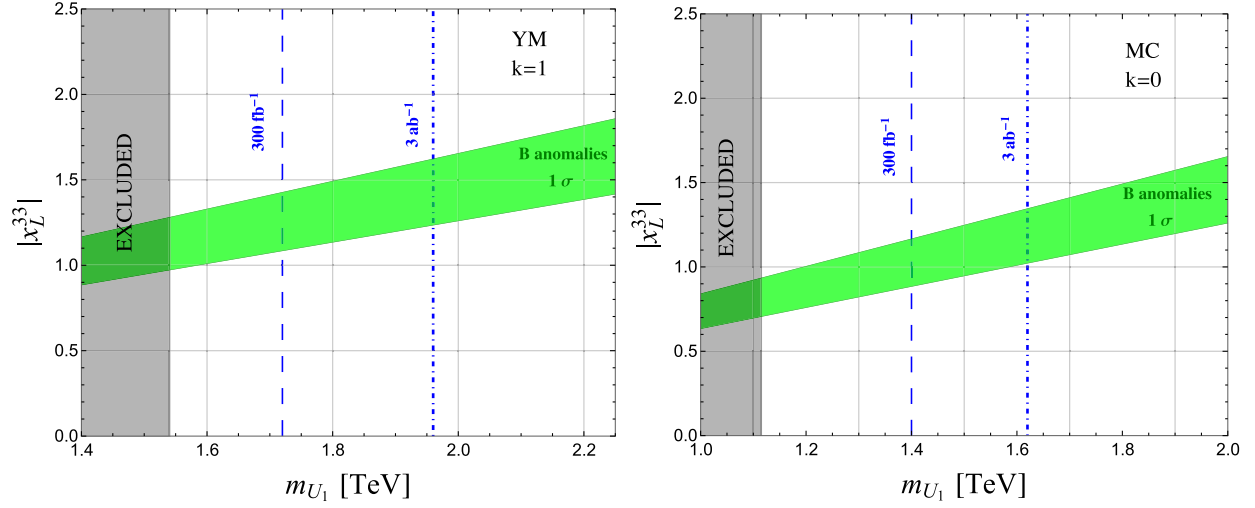
FIG. 7. Coupling vs mass parameter space for the vector LQ U_1 model preferred by B-physics anomalies compared to 95% C.L. limits obtained in our analysis in the $t\bar{t}$ plus missing energy channel. The green band is extracted from [40] and represents the 1σ region preferred by low-energy flavor observables, and the gray band indicates the current limit on m_{U_1}, from the CMS analysis [29] at $\sqrt{s} = 13$ TeV and 35.9 fb^{-1}. The blue lines are our lower bounds on the U_1 mass at $\sqrt{s} = 14$ TeV with a luminosity of 300 (dashed line) and 3000 (dotted line) fb^{-1}. The plot on the left (right) refers to the YM (MC) scenario.

The green band is extracted from [40] and represents the 1σ region preferred by low-energy flavor observables, and the gray band indicates the current limit on m_{U_1}, which comes from the CMS analysis [29] at $\sqrt{s} = 13$ TeV and 35.9 fb^{-1}. The blue lines are our lower bounds on the U_1 mass at $\sqrt{s} = 14$ TeV with a luminosity of 300 (dashed line) and 3000 (dotted line) fb^{-1}. We see that HL-LHC can probe in
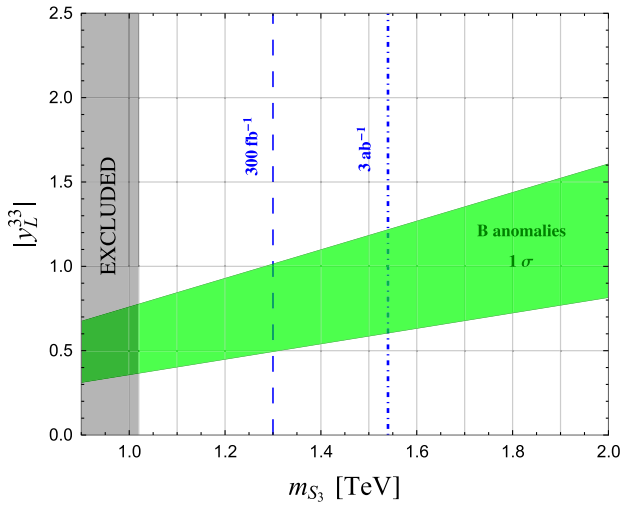

FIG. 8. Coupling vs mass parameter space for the scalar LQ S_3 model preferred by B-physics anomalies compared to 95% C.L. limits obtained in our analysis in the $t\bar{t}$ plus missing energy channel. The 1σ region preferred by low-energy flavor observables (green band) is extracted from [39], and the gray band indicates the current limit on m_{S_3}, from the CMS analysis [29] at $\sqrt{s} = 13$ TeV and 35.9 fb^{-1}. The blue lines are our lower bounds on the S_3 mass at $\sqrt{s} = 14$ TeV with a luminosity of 300 (dashed line) and 3000 (dotted line) fb^{-1}.

the $t\bar{t}\nu\nu$ channel a large part of the parameter space. Comparing with the projections presented in [40][10] for the reach in other channels, as $bb\tau\tau$, and production mechanisms, as single production, or in the dilepton tails, we can note that our analysis in the $t\bar{t}\nu\nu$ channel appears to be the most efficient to test models with LQs involved in the explanation of the flavor anomalies. If the HL-LHC program will exclude a LQ U_1 in the $t\nu$ channel, the B-physics anomalies can only be explained by considering large couplings $x_L^{33} > 1$.

Finally, we consider scalar LQs. Scalar LQs, either $SU(2)_L$ triplets, S_3, or singlets, S_1, are particularly motivated in scenarios with a BSM composite dynamics and can accommodate B anomalies [39,65]. In particular, S_3 is a good candidate to explain the anomaly in $R_{K^{(*)}}$ and S_1 the one in $R_{D^{(*)}}$ [64]. We focus on the model in [39]. From the $U(2)_q \times U(2)_\ell$ ansatz, the coupling in Eq. (2) reads $y_L^{ij} \equiv g_3\beta_{ij}$, with $\beta_{ij} = \delta_{3i}\delta_{3j}$. We show in Fig. 8 the part of the coupling vs m_{S_3} parameter space that can be probed by our results. The green band shows the 1σ flavor fit and is extracted from Ref. [39], the gray band indicates the current limit on m_{S_3} from the CMS analysis [29], and the blue lines indicate the 95% C.L. limits on the S_3 masses derived in our study. We see again that our analysis at the HL-LHC can probe a large portion of the parameter space relevant to B anomalies. We can also note, by comparing our results with the projected reach in different channels shown in Fig. 2 of

---

[10]Reference [40] only considers the MC scenario, but the relative sensitivities of the different channels remain the same in the YM case.

[39], that the $t\bar{t}\nu\nu$ channel is one of the most powerful to test the relevant parameter space for B anomalies.

VII. CONCLUSIONS

We have studied the pair production of LQs in the $t\bar{t}$ plus missing energy channel, which is one of the most powerful to detect third-generation LQs. These particles, as highlighted in the recent literature, offer an explanation to the B-physics flavor anomalies. We have indicated a search strategy in the channel, which shows the advantages of tagging the tops in the final state and which uses observables constructed out of the tops to discriminate the signal from the background and to characterize the signal. We have then assessed the reach on LQs of the future high-luminosity LHC program. Our results, presented in Fig. 4, show that with 3 ab^{-1} (300 fb^{-1}) the HL-LHC can exclude a vector LQ, in the YM scenario, and decaying 50% to top and neutrino, up to 1.96 TeV (1.72 TeV) or observe at 3σ the corresponding signal for masses up to 1.83 TeV (1.6 TeV). In the MC case, a vector LQ with a mass up to 1.62 TeV (1.4 TeV) can be excluded with 3 ab^{-1} (300 fb^{-1}). For the case of a scalar LQ completely decaying into top and neutrino, the exclusion reach extends up to 1.54 TeV (1.3 TeV) with 3 ab^{-1} (300 fb^{-1}), while scalar LQs as heavy as 1.41 TeV (1.16 TeV) can be observed at 3σ. We have further presented several observables, again constructed out of the tops, that, in case of a future discovery in the channel, can be used to distinguish between a scalar and a vector LQ (Figs. 5 and 6).

Finally, we have discussed the implications of our results to models addressing the recent B-physics anomalies. The search in the $t\bar{t}\nu\nu$ channel probes to be a very efficient test of these models, with the possibility to constrain a large part of the interesting parameter space (Figs. 7 and 8).

[1] J. C. Pati and A. Salam, Phys. Rev. D **10,** 275 (1974); **11,** 703(E) (1975).

[2] H. Georgi and S. L. Glashow, Phys. Rev. Lett. **32,** 438 (1974).

[3] G. M. Pelaggi, F. Sannino, A. Strumia, and E. Vigiani, Front. Phys. **5,** 49 (2017).

[4] S. Fajfer, J. F. Kamenik, I. Nisandzic, and J. Zupan, Phys. Rev. Lett. **109,** 161801 (2012).

[5] R. Alonso, B. Grinstein, and J. Martin Camalich, J. High Energy Phys. 10 (2015) 184.

[6] S. Fajfer and N. Košnik, Phys. Lett. B **755,** 270 (2016).

[7] R. Barbieri, G. Isidori, A. Pattori, and F. Senia, Eur. Phys. J. C **76,** 67 (2016).

[8] D. Bečirević, S. Fajfer, N. Košnik, and O. Sumensari, Phys. Rev. D **94,** 115021 (2016).

[9] Y. Cai, J. Gargalionis, M. A. Schmidt, and R. R. Volkas, J. High Energy Phys. 10 (2017) 047.

[10] M. Huschle et al. (Belle Collaboration), Phys. Rev. D **92,** 072014 (2015).

[11] S. Hirose et al. (Belle Collaboration), Phys. Rev. Lett. **118,** 211801 (2017).

[12] Y. Sato et al. (Belle Collaboration), Phys. Rev. D **94,** 072007 (2016).

[13] A. Abdesselam et al. (Belle Collaboration), arXiv:1603 .06711.

[14] J. P. Lees et al. (BABAR Collaboration), Phys. Rev. Lett. **109,** 101802 (2012).

[15] J. P. Lees et al. (BABAR Collaboration), Phys. Rev. D **88,** 072012 (2013).

[16] R. Aaij et al. (LHCb Collaboration), Phys. Rev. Lett. **115,** 111803 (2015); **115,** 159901(E) (2015).

[17] R. Aaij et al. (LHCb Collaboration), Phys. Rev. Lett. **113,** 151601 (2014).

[18] R. Aaij et al. (LHCb Collaboration), J. High Energy Phys. 08 (2017) 055.

[19] L. Di Luzio and M. Nardecchia, Eur. Phys. J. C **77,** 536 (2017).

[20] M. Bauer and M. Neubert, Phys. Rev. Lett. **116,** 141802 (2016).

[21] D. Das, C. Hati, G. Kumar, and N. Mahajan, Phys. Rev. D **94,** 055034 (2016).

[22] A. Crivellin, D. Müller, and T. Ota, J. High Energy Phys. 09 (2017) 040.

[23] R. N. Mohapatra, G. Segre, and L. Wolfenstein, Phys. Lett. **145B,** 433 (1984).

[24] I. Doršner, S. Fajfer, A. Greljo, J. F. Kamenik, and N. Košnik, Phys. Rep. **641,** 1 (2016).

[25] I. Doršner and A. Greljo, J. High Energy Phys. 05 (2018) 126.

[26] B. Diaz, M. Schmaltz, and Y. M. Zhong, J. High Energy Phys. 10 (2017) 097.

[27] A. Greljo and D. Marzocca, Eur. Phys. J. C **77,** 548 (2017).

[28] CMS Collaboration, Report No. CMS-PAS-B2G-16-027.

[29] A. M. Sirunyan et al. (CMS Collaboration), Phys. Rev. D **98,** 032005 (2018).

[30] CMS Collaboration, Report No. CMS-PAS-EXO-17-016.

[31] A. M. Sirunyan et al. (CMS Collaboration), J. High Energy Phys. 07 (2017) 121.

[32] A. M. Sirunyan *et al.* (CMS Collaboration), Eur. Phys. J. C **78,** 707 (2018).

[33] M. Aaboud *et al.* (ATLAS Collaboration), New J. Phys. **18,** 093016 (2016).

[34] CMS Collaboration, Report No. CMS-PAS-EXO-17-029.

[35] T. Golling *et al.*, arXiv:1606.00947.

[36] B. C. Allanach, B. Gripaios, and T. You, J. High Energy Phys. 03 (2018) 021.

[37] G. Hiller, D. Loose, and I. Nišandžić, Phys. Rev. D **97,** 075004 (2018).

[38] B. Dumont, K. Nishiwaki, and R. Watanabe, Phys. Rev. D **94,** 034001 (2016).

[39] D. Marzocca, J. High Energy Phys. 07 (2018) 121.

[40] D. Buttazzo, A. Greljo, G. Isidori, and D. Marzocca, J. High Energy Phys. 11 (2017) 044.

[41] A. Biswas, D. Kumar Ghosh, N. Ghosh, A. Shaw, and A. K. Swain, arXiv:1808.04169.

[42] W. Buchmuller, R. Ruckl, and D. Wyler, Phys. Lett. B **191,** 442 (1987); **448,** 320(E) (1999).

[43] D. Bečirević, I. Doršner, S. Fajfer, D. A. Faroughy, N. Košnik, and O. Sumensari, Phys. Rev. D **98,** 055003 (2018).

[44] J. Alwall, R. Frederix, S. Frixione, V. Hirschi, F. Maltoni, O. Mattelaer, H.-S. Shao, T. Stelzer, P. Torrielli, and M. Zaro, J. High Energy Phys. 07 (2014) 079.

[45] T. Sjostrand, S. Mrenna, and P. Z. Skands, J. High Energy Phys. 05 (2006) 026.

[46] S. Ovyn, X. Rouby, and V. Lemaitre, arXiv:0903.2225.

[47] C. Degrande, C. Duhr, B. Fuks, D. Grellscheid, O. Mattelaer, and T. Reiter, Comput. Phys. Commun. **183,** 1201 (2012).

[48] N. D. Christensen and C. Duhr, Comput. Phys. Commun. **180,** 1614 (2009).

[49] T. Mandal, S. Mitra, and S. Seth, Phys. Rev. D **93,** 035018 (2016).

[50] R. D. Ball, V. Bertone, S. Carrazza, L. Del Debbio, S. Forte, A. Guffanti, N. P. Hartland, and J. Rojo (NNPDF Collaboration), Nucl. Phys. **B877,** 290 (2013).

[51] M. Cacciari, G. P. Salam, and G. Soyez, Eur. Phys. J. C **72,** 1896 (2012).

[52] M. Cacciari, G. P. Salam, and G. Soyez, J. High Energy Phys. 04 (2008) 063.

[53] A. M. Sirunyan *et al.* (CMS Collaboration), J. High Energy Phys. 01 (2018) 097.

[54] S. Marzani, L. Schunk, and G. Soyez, J. High Energy Phys. 07 (2017) 132.

[55] G. Aad *et al.* (ATLAS Collaboration), J. High Energy Phys. 10 (2013) 189.

[56] A. M. Sirunyan *et al.* (CMS Collaboration), Eur. Phys. J. C **77,** 710 (2017).

[57] J. Thaler and K. Van Tilburg, J. High Energy Phys. 03 (2011) 015.

[58] I. W. Stewart, F. J. Tackmann, and W. J. Waalewijn, Phys. Rev. Lett. **105,** 092002 (2010).

[59] M. R. Buckley, S. Y. Choi, K. Mawatari, and H. Murayama, Phys. Lett. B **672,** 275 (2009).

[60] M. R. Buckley and D. Goncalves, Phys. Rev. D **93,** 034003 (2016).

[61] U. Haisch, P. Pani, and G. Polesello, J. High Energy Phys. 02 (2017) 131.

[62] J. Ellis, D. S. Hwang, K. Sakurai, and M. Takeuchi, J. High Energy Phys. 04 (2014) 004.

[63] F. Demartin, F. Maltoni, K. Mawatari, B. Page, and M. Zaro, Eur. Phys. J. C **74,** 3065 (2014).

[64] A. Angelescu, D. Bečirević, D. A. Faroughy, and O. Sumensari, J. High Energy Phys. 10 (2018) 183.

[65] B. Gripaios, M. Nardecchia, and S. A. Renner, J. High Energy Phys. 05 (2015) 006.